Korean J. Chem. Eng., 39(3), 655-663 (2022)
DOI: 10.1007/s11814-021-0969-z

pISSN: 0256-1115
eISSN: 1975-7220

Calcium precipitation to remove fluorine in groundwater: Induced by *Acinetobacter* sp. H12 as a template

Junfeng Su*,,†, Ruijie Zhang*,**, Xiaofen Hu*,**, Amjad Ali*,**, and Zhao Wang*,****

*School of Environmental and Municipal Engineering, Xi'an University of Architecture and Technology, Xi'an 710055, China
**Shaanxi Key Laboratory of Environmental Engineering, Xi'an University of Architecture and Technology, Xi'an 710055, China
(*Received 18 April 2021 • Revised 11 September 2021 • Accepted 29 September 2021*)

Abstract−Calcium precipitation induced by *Acinetobacter* sp. H12 can simultaneously remove F^- and Ca^{2+}. Adsorption kinetics and isotherm studies showed that the defluoridation effect improved with the increase of temperature and time. The equilibrium adsorption capacity of calcium precipitation was 7.43 mg g^{-1} at the initial F^- concentration of 10 mg L^{-1}. Moreover, as the pH increased, the F^- adsorption capacity decreased and the Ca^{2+} removal rate gradually increased. The adsorption process was highly fitted to the pseudo-second-order and the Freundlich isotherm. Adsorption thermodynamics analysis demonstrated that the adsorption process was a spontaneous endothermic reaction. The activation adsorption energy was 2.81 kJ mol^{-1} and the frequency coefficient was 10.88 h^{-1}. EEM, SEM, XPS. XRD results indicated that the defluoridation mechanism may be due to adsorption and co-precipitation. The mechanism of Ca^{2+} removal may be co-precipitation with F^-. It is worth-mentioning that calcium precipitation overcame the problem of adding carbon sources and avoided the microbial safety risk in the effluent. Therefore, a new insight was proposed for simultaneous remediation of Ca^{2+} and F^- from groundwater combining the biological and chemical method.

Keywords: Biomineralization, Defluoridation, Kinetics, MICP, Thermodynamics

INTRODUCTION

More than 50% of the global population uses groundwater for drinking [1]. However, in many countries in Africa and Asia, the fluoride (F^-) concentration in groundwater exceeds the permissible limit (1.5 mg L^{-1}) of the World Health Organization [2,3]. Drinking of groundwater with excessive F^- for a long period will damage human health as well as lead to dental or skeletal fluorosis [4,5]. Excessive F^- would lead to alterations in tooth enamel, which causes staining and pitting. More seriously, high levels of F^- may affect brain and nerve cells [6]. Therefore, the removal of F^- from groundwater is indispensable in terms of environmental safety and human health. The main methods to remove excessive F^- are adsorption, coagulation/precipitation, electrodialysis, ion exchange, and reverse osmosis [2,7]. The adsorption method, due to its mature technology, convenient operation, low operating cost, and good adsorption effect, has been widely used for defluoridation [8,9,10]. In addition, the precipitation method does not require any equipment but also has a good defluoridation effect [11].

Calcium (Ca^{2+}) is an alkaline earth metal widely found in natural and industrial water bodies. More than 97% of global runoff is affected by the dissolution of $CaCO_3$, resulting in water hardness usually related to alkalinity in aquatic ecosystems [12]. Although the amount of Ca^{2+} in drinking water does not pose any serious health problems, it can cause scaling and make detergents and soaps less effective at cleaning [13]. Common techniques for removing Ca^{2+} from water consist of ion exchange, adsorption, and filtration [14]. Although these processes have simple operation, strong absorption capacity, and easy manufacturing, they also cause many problems, such as higher initial costs, excessive waste, and consumption of hydropower [15]. Biological treatment processes, by contrast, are considered eco-friendly and economical, which has garnered growing research interest. The application of biological methods to induce crystallization combined with chemical adsorption overcomes a wide variety of shortcomings in the traditional process, which is greatly propitious for water remediation [16].

Biomineralization is the deposition of a mineral caused by environmental chemical changes due to microbial activities [17]. It is a common phenomenon in nature, inducing the formation of over sixty different biominerals [18]. Biomineralization has been widely concerned by experts in the field of chemistry, physics, biology, materials, medicine, life science, and environment. Microbial induced carbonate precipitation (MICP) is a biomineralization process that is widely existing in nature [19]. MICP is the precipitation of calcium carbonate owing to the existence of microorganisms and their biochemical activity in a supersaturated solution [20,21]. First, microorganisms produce many carbonates when they consume organic matter [22]. Secondly, because the microbial surface is negatively charged and the Ca^{2+} is positively charged, much Ca^{2+} is accumulated on the surface of the microbial cells [23]. They combine with carbonate in a supersaturated solution to form calcium carbonate [24]. Moreover, microorganisms have negatively charged carboxyl groups, phosphates, and amines on their surface in combination with Ca^{2+}, which are favorable sites for nucleation of calcium carbonate [25].

Compared with the previous methods [26], the calcium precip-

†To whom correspondence should be addressed.
E-mail: sjf1977518@sina.com

itation method we adopted combines adsorption and precipitation. On the one hand, F^- adsorbs and removes by calcium precipitation. On the other hand, the combination of F^- and Ca^{2+} makes the precipitation continue to grow, and Ca^{2+} is removed due to co-precipitation. Microbes act as nucleation centers when they induce calcium precipitation. Ca^{2+} is attracted by the negative charges surrounding the microorganisms and combines with other ions in the water to form a precipitate. Therefore, calcium precipitation, as a kind of adsorbent and seed crystal, will continue growth through co-precipitate and adsorb [27].

Acinetobacter sp. H12 was used to induce calcium precipitation and effectively removed F^- and Ca^{2+} in contaminated water. Calcium precipitation is a seed crystal for biologically induced synthesis. The biggest advantage is that calcium precipitation overcomes the problem of adding carbon sources in underground water treatment and reduces the risk of excess water organisms. Compared with other methods, it has the advantages of green environmental protection, simplicity and practicality, and remarkable effects. In this study, calcium carbonate precipitation caused by *Acinetobacter* sp. H12 was collected in the early stage of nucleation. The calcium precipitation removes F^- and Ca^{2+} through MICP. The adsorption kinetics model of F^- was established by using the pseudo-first-order and pseudo-second-order rate equations. Thermodynamic parameters were obtained through adsorption isotherm experiments and thermodynamic experiments to define the type of adsorption. The effect of pH on the simultaneous removal of F^- and Ca^{2+} was also discussed. The fluorescence excitation-emission matrix spectra (EEM), scanning electron microscopy (SEM), X-ray photoelectron spectroscopy (XPS), and X-ray diffraction (XRD) were used to study the characterization and removal mechanism.

MATERIALS AND METHODS

1. Culture Medium Preparation

The sources of biomineralized bacteria H12 were the rock surface sediment from Qu Jiang artificial lake, Shaanxi Province, China [28]. According to our previous research, strain H12 can induce calcium precipitation and remove nitrate through aerobic denitrification.

The basic medium (BM) used in this investigation comprised the following reagents: $C_4H_4Na_2O_4{\cdot}6H_2O$ (0.5 g L^{-1}), $NaNO_3$ (0.1 g L^{-1}), KH_2PO_4 (0.05 g L^{-1}), $MgSO_4{\cdot}7H_2O$ (0.05 g L^{-1}), $CaCl_2$ (0.5 g L^{-1}) [29]. Sodium fluoride (NaF) was added to distilled water to make a concentrated F^- stock solution of 1 mg mL^{-1}. The F^--free BM was sterilized at 121 °C in an autoclave for 30 minutes. F^- stock solution was added to BM, cooled to 26 °C and initial pH was adjusted to 7. Then, a 200 mL conical flask containing strain H12 and 150 mL of medium was cultured in a constant temperature incubator. During the whole experiment, the reactor temperature was kept at 30 °C under aerobic conditions and the rotation speed was 145 rpm [30].

The solution was incubated at 30 °C for calcium precipitation for 36 to 48 hours. The removed precipitate was separated at 8,000 rpm through a centrifuge and washed with deionized water. Powder samples were obtained after drying for 24 hours at 50 °C in an oven [31].

2. Fluoride Adsorption Kinetics and Isotherm Experiments

The kinetics of the adsorption process can be fitted with many models, such as pseudo-first-order kinetics models and pseudo-second-order kinetic models [5,10,32]. The adsorption isotherm can be used to describe the adsorption equilibrium of F^-. The adsorption isotherm shows the relationship of equilibrium concentration and adsorption capacity of F^- adsorbed by calcium precipitation change with temperature [33]. The equations of kinetics and isotherm models are presented in Table S1.

3. Fluoride Adsorption Thermodynamics Experiments

According to the van't Hoff equation, Eqs. (1), (2), and (3) can be used to obtain the change in Gibbs free energy (ΔG), change in enthalpy (ΔH), and change in entropy (ΔS), respectively, during the adsorption process [34-36]. Adsorption type is determined through these thermodynamic parameters. Moreover, the Arrhenius equation (Eq. (4)) can determine the activation energy and the adsorption rate constant of the process.

$$\Delta G = -RT\ln K \quad (1)$$

$$\Delta G = \Delta H - T\Delta S \quad (2)$$

$$\ln K = -(\Delta H/RT) + (\Delta S/R) \quad (3)$$

$$\ln K = \ln A - Ea/RT \quad (4)$$

where, T is the temperature, K is the equilibrium adsorption constant, R is the universal gas constant, A is the frequency factor (h^{-1}) and Ea is the activation energy (kJ mol^{-1}).

4. Characterization and Analysis Methods

Calcium precipitation was characterized through centrifugal separation experiments of biological precipitation at different stages. Zeta potential was recorded using a Zeta size instrument (Nano ZS90, Malvern, UK) at pH of 6.0, 7.0, 8.0. Biological precipitates in the F^--free group and the F^--added group were analyzed by SEM (JSM-6510LV, Japan JEOL), XPS (Kratos AXIS Ultra, UK), XRD (Rigaku, Japan), and EEM during MICP measured by F-7000 fluorescence spectrophotometer (Hitachi Co., Japan).

The concentration of F^- and Ca^{2+} was measured by fluoride electrode (PXSJ-216F, Shanghai, China) and flame atomic absorption spectrometry (ICP-1100, Thermo, USA). The pH values of the samples were determined by pH meter (HQ11d, HACH, USA). The adsorption efficiency (%) was calculated by $(Q_0 - Q_n)/Q_0$, where Q_0 and Q_n were the initial and final adsorption concentration (mg g^{-1}) [11].

RESULTS AND DISCUSSION

1. Formation and Removal Capacity of Calcium Precipitation

As we know, MICP is a type of biomineralization. According to our previous research, strain H12 has the ability of MICP [27]. The strain H12 was added into the BM and cultured at 30 °C under aerobic conditions. The solution gradually produced calcium precipitate under the action of MICP. Calcium precipitation cultured for 36-48 hours was taken out and added into a supersaturated solution containing F^-. The 1.0 g L^{-1} calcium precipitation species was put into the actual groundwater containing F^- (actual groundwater was taken from Guodu Town, Chang'an District, Shaanxi

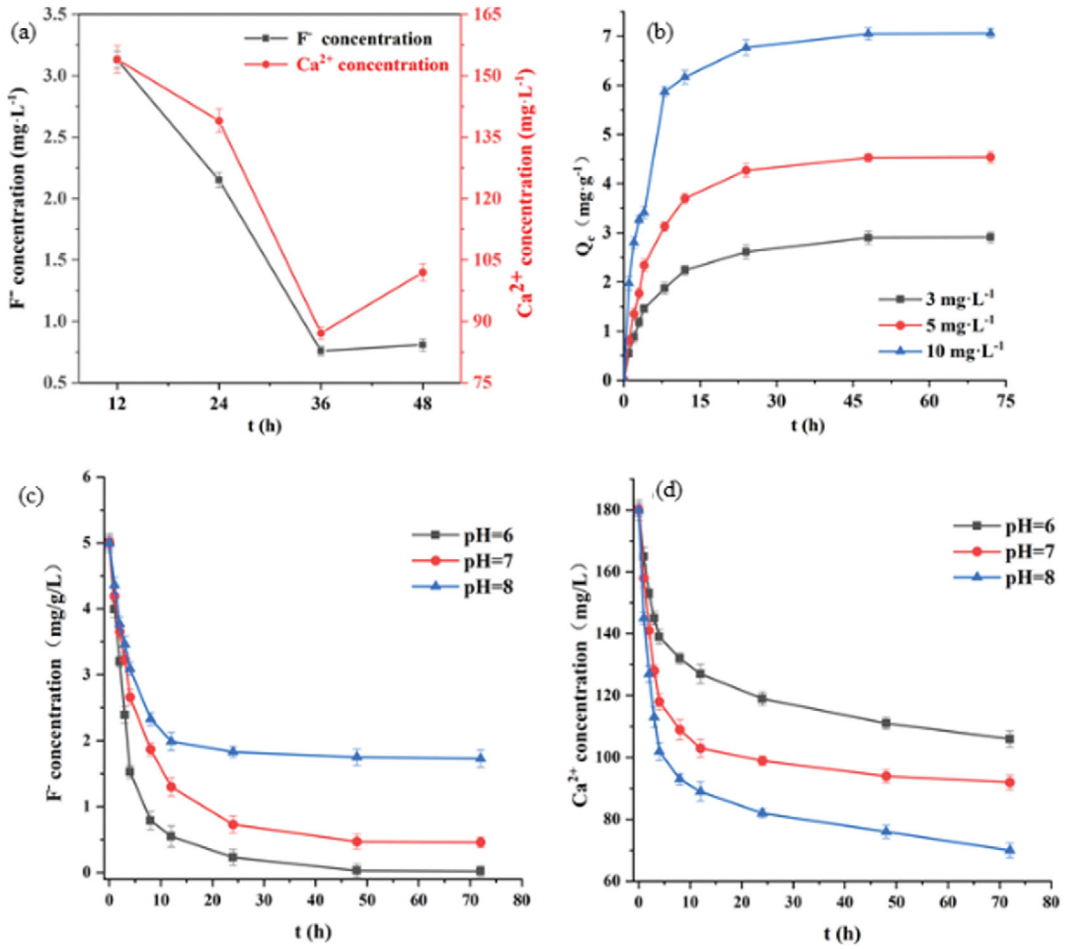

Fig. 1. Removal capacity in calcium precipitation prepared at different times (a); the change of adsorption capacity at initial F^- concentration (b); removal effect of different pH values on F^- (c) and Ca^{2+} (d).

Province, China). The concentration of F^- was 3 mg L^{-1} and Ca^{2+} was 180 mg L^{-1}. After the shock test at 48 h, 30 °C and 145 rpm, the residual concentrations of F^- and Ca^{2+} (Fig. 1(a)) seemed that the calcium precipitation induced by strain H12 obtained at 36 h had the best effect, where the residual concentrations of F^- and Ca^{2+} were 0.76 and 87.14 mg L^{-1}, respectively.

The results illustrated that F^- was adsorbed and removed by the calcium precipitation obtained after 36 h, and the Ca^{2+} was removed simultaneously in the supersaturated medium containing F^- induced by strain H12. The process of biomineralization is generally regarded as the principle of crystal nucleation [37]. First, the negative charge on the surface of microorganisms attracts Ca^{2+} in the water. Moreover, the metabolism of microorganisms may cause variation in the alkalinity of water, leading to increased CO_3^{2-} and OH^- concentrations. Finally, CO_3^{2-} and OH^- will combine with Ca^{2+} on the surface of the microorganisms to form a precipitate [26]. Nucleation, the first step of the crystallization process, is also the most critical, which will affect many important characteristics of the crystal. The bacteria are taken as the core to produce the crystal nucleus, that is, the calcium precipitation, exhibiting loose and porous properties in the early stages of nucleation [38]. With the increase of culture time, the biomass was gradually enriched, a larger adsorption capacity and more adsorption sites were also created. Compared with the 48-hour biological precipitation, there were more sites that did not bind with calcium ions, which was more conducive to the subsequent removal of F^- and Ca^{2+} in the water. Zhu [39] proved that the efficiency of microorganisms to induce calcium precipitation is 2.6 times higher than that under non-biological conditions. In addition, the calcium precipitate induced by microorganisms is larger than that produced under abiotic conditions. In summary, the calcium precipitation induced by strain H12 has the characteristics of large yield and high speed. Since calcium precipitation has more nucleation sites in the early stage of nucleation, it may have a strong ability to remove F^- and Ca^{2+}.

The change in adsorption capacity of calcium precipitation under different initial F^- concentration with time is shown in Fig. 1(b). The adsorption process of F^- by calcium precipitation can be divided into rapid adsorption, slow adsorption, and equilibrium phase. The adsorption rate of adsorbent in the first 4 h was very high, and the adsorption amount reached about 50% of the equilibrium adsorption amount. The adsorption rate decreased after 4 h. After 24 h, little change in the adsorption capacity was observed and then reached equilibrium. The early rapid adsorption may be due to the larger concentration differences and more available

adsorption sites. As the reaction time increased, the concentration differences in the solution and the nucleation sites of calcium precipitation gradually decreased. The later adsorption process gradually became slower, which may be due to physical adsorption mainly occurring in the initial stage [32]. After physical adsorption, a chemical adsorption process such as ion exchange may occur to achieve further removal of F^-. In summary, the increase in initial F^- concentration can accelerate the adsorption rate. After the rapid adsorption phase is completed, the rate slows until adsorption equilibrium.

We speculate that calcium precipitation can remove fluoride in two ways: (i) F^- are adsorbed by calcium precipitation, and (ii) F^- are co-precipitated with Ca^{2+}. As mentioned, calcium precipitation retains the characteristics of seed crystal and can continue to induce precipitation while adsorbing. Therefore, it is possible that the removal of F^- is inseparable from these two methods. Moreover, after calcium precipitation treatment, the groundwater can be quickly removed by filtration and the risk of effluent organisms can be reduced.

2. Effect of pH Value on the Removal of F^- and Ca^{2+}

The F^- removal effects of different pH on calcium precipitation in water are shown in Fig. 1(c). The adsorption capacity of F^- to calcium precipitation decreased with the increasing pH. The maximum adsorption capacity was 5.22 mg g^{-1} when the pH value was 6. In acidic media, the surface of calcium precipitation is highly protonated and has a positive charge. Therefore, the positively charged calcium precipitate on the surface may more easily absorb F^-. The content of OH^- increased with increasing the solution pH. Although F^- has more affinity than OH^-, when the OH^- concentration is high, OH^- and F^- have strong competition for adsorptive sites, and the removal rate of F^- decreases. The adsorption capacity of calcium precipitation decreased due to the presence of OH^- at higher pH, the F^- became highly electronegative and repelled negatively charged OH^- [40].

Fig. 1(d) shows that the Ca^{2+} removal rate gradually increased as the pH value increased from 6.0 to 9.0. When the pH was 9.0, the maximum removal ratio was 61.11%. The Ca^{2+} concentration decreased from the initial 180 to 70 mg L^{-1}. The results illustrated that the alkaline environment was favorable for Ca^{2+} removal. Compared with acidic conditions, Ca^{2+} has lower solubility under alkaline conditions. When the pH was high, it favored the HCO_3^- in the solution to convert to CO_3^{2-} and thus combine with Ca^{2+} to form precipitation [41]. Most calcite will be precipitated under the alkaline condition of pH 8.7-9.5 [42]. However, the carbonate dissolves rather than precipitates at a low pH. Thus, acidic conditions are not conducive to the growth of calcium precipitation. In summary, the Ca^{2+} removal rate increases with the increasing pH.

It can be seen from the Fig. S1 that the zeta potentials of the calcium precipitation have negative charges under different pH conditions, creating an environment of attracting calcium ions continually. New crystals were formed on the surface of calcium precipitation, which also produced greater adsorption capacity and more adsorption sites. Thus, it can be considered that the zeta potential of the calcium precipitation is nearly independent on defluoridation. Consistent with the previously described conclusion, the removal of fluoride is more based on chemical adsorption rather than electrostatic attraction. Meanwhile, crystals also promote co-precipitation of calcium and fluorine.

3. Fluorescence Spectroscopy During MICP

The degree of biological metabolism was measured by exci-

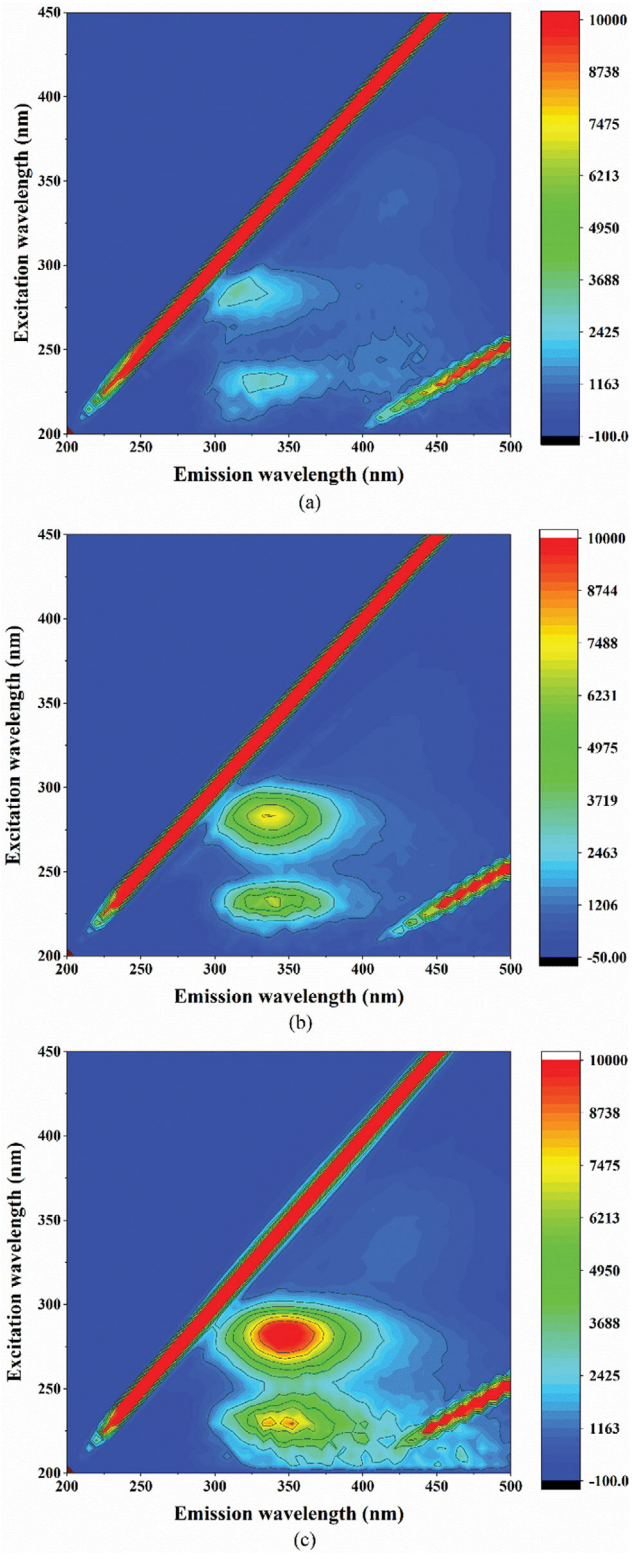

Fig. 2. Excitation-emission matrix spectra of the samples at 6 (a), 12 (b), and 24 h (c).

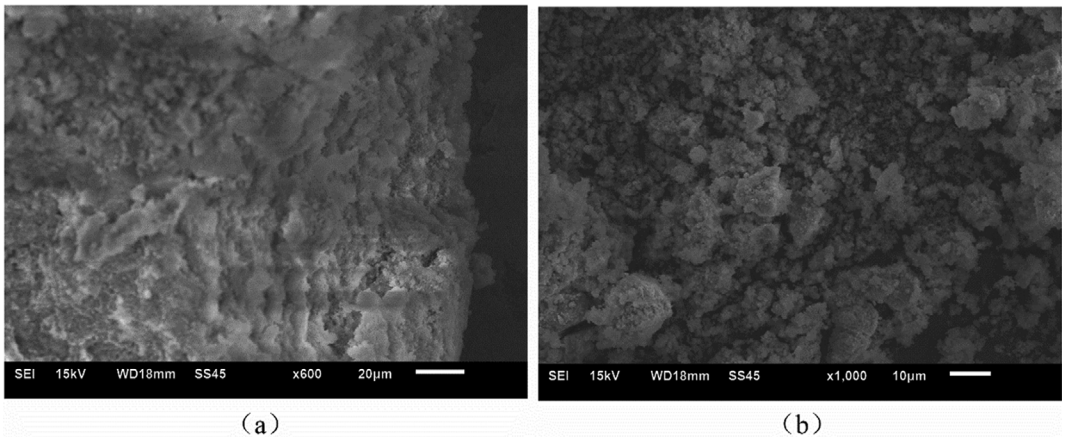

Fig. 3. Scanning electron microscopy of formation of calcium precipitation (a), and calcium precipitation aggregation (b).

tation-emission matrix fluorescence spectrometry (Fig. 2). The EEM spectrum was delineated into four regions. Region I (EX <250 nm, EM <380 nm), Region II (EX <250 nm, EM >380 nm), Region III (EX 250-280 nm, EM <380 nm), and Region IV (EX >280 nm, EM >380 nm) are related to simple aromatic proteins, soluble microbial by-products, fulvic acid-like, and humic acid-like substances, respectively [29]. The concentration of fluorescent substances is usually qualitatively analyzed by fluorescence peak intensity (FI). The peak area increases when fluorescent substances are more. The two peaks in Fig. 2 represent aromatic protein and tryptophan protein [29]. The metabolites produced by strain H12 contain carboxyl, phosphate, and hydroxyl groups. These negatively charged groups provide more nucleation sites which generate exchange sites, providing adsorption capacity [43]. We can see that the peak area increases with time. In conclusion, it demonstrated that the MICP based on denitrifying bacteria requires a certain reaction time to produce metabolites which serve as nucleation sites during the adsorption process. These findings suggested that the biological metabolism of H12 strain plays a crucial role in the simultaneous removal of F^- and Ca^{2+} [27].

4. Mechanistic Analysis of Bio-precipitation

Fig. 3 describes the surface morphology changes of calcium precipitation. The surface morphology of biological precipitate was collected before and after the adsorption and characterized by SEM. As shown in Fig. 3(a), the bacteria was covered on the calcium precipitation. Fig. 3(b) shows that the calcium precipitation coating bacteria added to the water containing F^- and Ca^{2+} and it can be seen that the precipitation increased obviously. With the adhesion of F^- and Ca^{2+} on the surface of calcium precipitation, the aggregates formed changed significantly. In Fig. 3(a), the surface morphology of calcium precipitation is loose and porous. Fig. 3(b) shows the aggregate and deposit in large amounts occurring on the calcium precipitation surface after F^- adsorption. This is consistent with previous study of Su et al. [27]. We demonstrate that in the early stage of nucleation, the bacterial cell concentration is large and the calcium precipitation on the surface of the bacteria does not completely enclose the entire bacterial cell, so the calcium precipitation particles are fine and loose. This feature is very advantageous for adsorption. It illustrates that the removal of F^- and Ca^{2+} by calcium precipitation may be related to co-precipitation after the adsorption process. This is also consistent with some of the results of the adsorption kinetics (section 3.5).

The mechanism of calcium precipitation removal of F^- and Ca^{2+} was studied using XPS and XRD. The XPS results of nonfluorinated and fluorinated are shown in Fig. 4(a) and (b), respectively. In Fig. 4(b), the spectrum of F^- is visible where the distribution peak value is 684.08 eV. A typical F1s peak in Fig. 4(b) but not in Fig. 4(a) indicates that F^- was absorbed through the calcium pre-

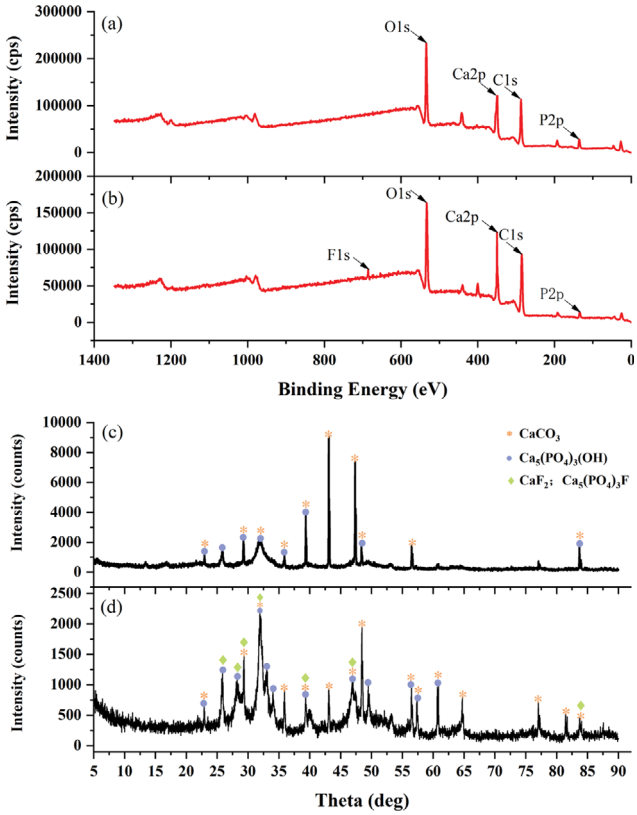

Fig. 4. XPS of precipitates without (a) and with (b) F^- loaded (All surveys) and XRD of precipitates without (c) and with (d) F^- loaded (All surveys).

cipitation. At the same time, it can be observed that the typical peak of Ca^{2+} at 350.08 eV heightened, which may indicate that the Ca^{2+} content had increased. Moreover, Fig. 4(c) and Fig. 4(d) show the XRD patterns of nonfluorinated and fluorinated sediments. The peak spectrum was acquired by X-ray diffraction on the surface of calcium precipitation. In Fig. 4((c) and (d)), the low-intensity peak indicates poor mineral crystallinity; otherwise, the mineral crystallinity is high in case [27]. In Fig. 4(c), typical peaks of $CaCO_3$ and $Ca_5(PO_4)_3OH$ are visible. In Fig. 4(d), in addition to $CaCO_3$ and $Ca_5(PO_4)_3OH$, the typical peaks of $Ca_5(PO_4)_3F$ and CaF_2 can also be observed. The metabolic activity of bacteria H12 in calcium precipitation changed the pH and CO_3^{2-} concentration in the environment, which indirectly affected the removal of F^- and Ca^{2+}. The existence of $CaCO_3$ and $Ca_5(PO_4)_3OH$ may be the precipitated components generated by calcium precipitation, which played a role in the removal of Ca^{2+}. The presence of CaF_2 indicates that the removal of F^- maybe due to the adsorption of Ca^{2+} on the surface of the bacteria. The presence of $Ca_5(PO_4)_3F$ and CaF_2 also confirms that the adsorption process described here may include chemical adsorption such as ion exchange. In $Ca_5(PO_4)_3OH$, the higher affinity of F^- may replace OH^-, causing chemical adsorption. According to our previous finding, four factors are associated with F^- removal mechanisms: (i) Ca^{2+} concentration, (ii) pH, (iii) CO_3^{2-} concentration, and (iv) the presence of nucleation sites [27]. Bacterial metabolism affects the content of the last three substances in the environment. Negative groups in the EPS secreted by bacteria can serve as nucleation sites [26] and bind to Ca^{2+} in a supersaturated solution, which will continue to induce the formation of precipitate to achieve Ca^{2+} removal. The mechanism of defluoridation is confirmed through EEM, SEM, XPS, and XRD.

According to the removal mechanism, strain H12 induced the formation of calcium precipitation, which was removed at the initial stage of nucleation and then added into a supersaturated solution containing F^-. On the one hand, the loose and porous calcium precipitates will adsorb F^-. On the other hand, Ca^{2+} and F^- in the water co-precipitate to produce CaF_2. Calcium precipitation, which is an adsorbent for F^-, will continue to increase due to the appearance of CaF_2. Therefore, the mechanism of F^- removal was due to adsorption and co-precipitation and the mechanism of Ca^{2+} removal was by co-precipitation.

5. Adsorption Kinetics and Isotherm Analysis of F^- Removal

Fig. 5 shows that the fitting degree of the pseudo-second-order kinetics model was higher than that of pseudo-first-order kinetics model under different initial F^- concentration and pH conditions (initial F^- concentration at 3, 5, and 10 mg·L^{-1}; pH at 6, 7, and 8; temperature at 30 °C). The kinetics experimental data are presented in Table 1. The correlation coefficient (R^2) of the pseudo-second-order kinetics model was greater than 0.99, indicating that the adsorption and removal of F^- by calcium precipitation may be a pseudo-second-order kinetics reaction [31]. The pseudo-second-

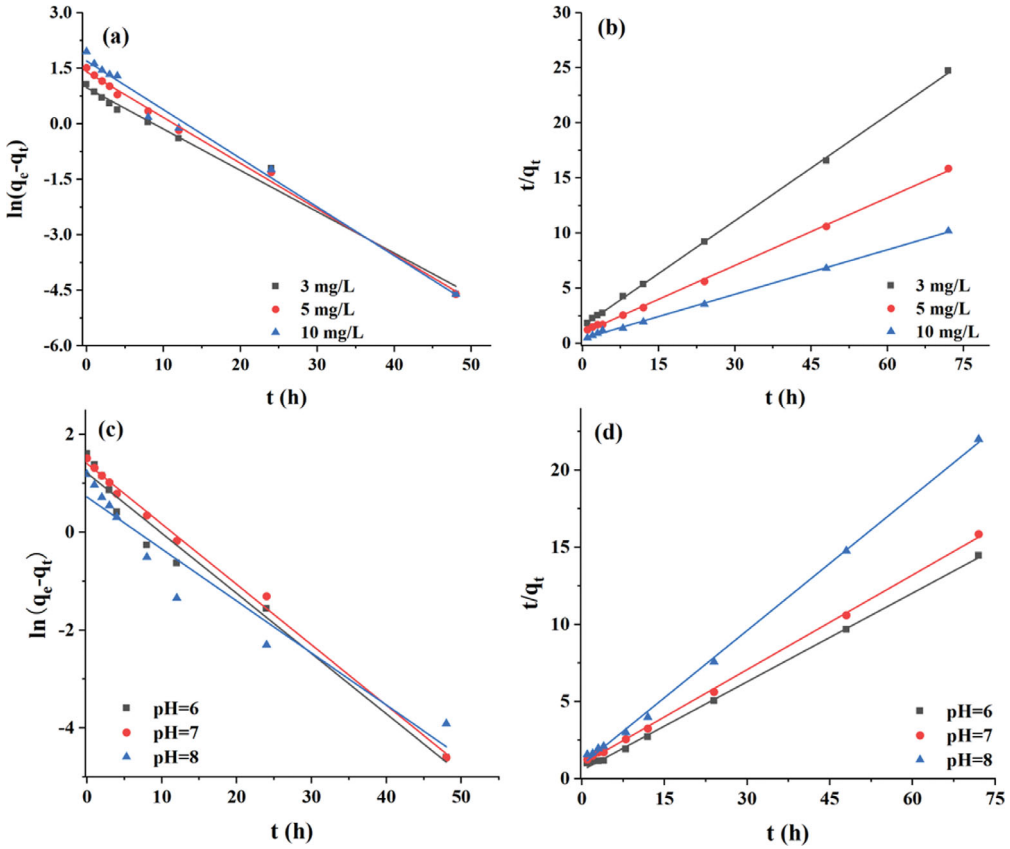

Fig. 5. Adsorption kinetics of fluoride by calcium precipitation: the pseudo-first-order kinetic model (a) the pseudo-second-order kinetic model (b) with different initial fluorine concentrations; the pseudo-first-order kinetic model (c) the pseudo-second-order kinetic model (d) with different initial pH.

Table 1. Calcium precipitation adsorption under different initial F^- concentrations and pH of dynamic parameters

Initial value		Pseudo-first-order			Pseudo-second-order		
		k_1	Q_e	R^2	k_2	Q_e	R^2
F^- (mg L^{-1})	3	0.1118	0.9766	0.9861	0.0657	3.1328	0.9996
	5	0.1236	1.4068	0.9963	0.0449	4.8876	0.9991
	10	0.1316	1.6997	0.9880	0.0434	7.4294	0.9988
pH	6	0.1232	1.2129	0.9742	0.0690	5.2165	0.9988
	7	0.1236	1.4068	0.9963	0.0449	4.8876	0.9991
	8	0.1064	0.7220	0.9320	0.0946	3.4423	0.9987

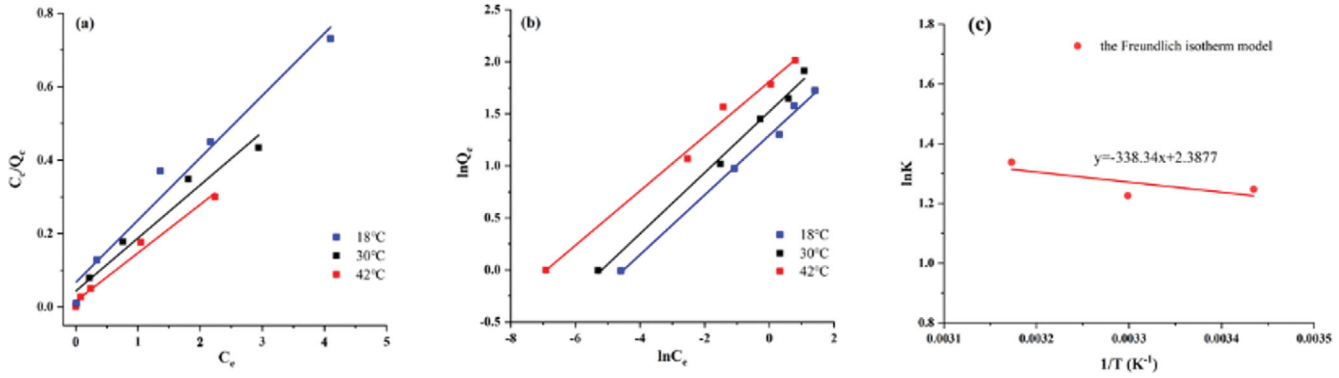

Fig. 6. Adsorption isotherm of fluoride by calcium precipitation: Langmuir isotherm model (a) and the Freundlich isotherm model (b); fitting curve between ln k and 1/T according to Arrhenius equation(c).

Table 2. Calcium precipitation adsorption under different temperature of dynamic parameters

Temperature (°C)	Langmuir			Freundlich		
	Q_m	K_A	R^2	k_f	n	R^2
18	15.55	0.18	0.7876	2.73	1.16	0.9937
30	7.49	1.93	0.9555	4.25	2.35	0.9900
42	1.01	61.65	0.9864	6.11	3.81	0.9902

order kinetics model considers three different processes in the adsorption process: (i) surface adsorption reaction, (ii) liquid film diffusion, and (iii) internal diffusion, which can better describe the entire adsorption process [10]. The larger the initial F^- concentration, the smaller the pseudo-second-order rate constant K_2. This may be ascribed to low concentration, as F^- has little competition for adsorption sites on the adsorbent surface and the adsorption rate is higher [44]. Although the concentration difference increases, the adsorption constant K_2 decreases. We illustrated that the increased adsorption driving force due to the increased concentration may be weaker than the adsorption force at the adsorption site. However, under the condition of high concentration, the adsorption rate decreases due to the strong competition of adsorption sites on the adsorbent surface. This also demonstrated that the F^- adsorption process may not be single physical adsorption, and the rate-limiting step may be related to chemical adsorption processes such as the exchange of electrons between the adsorbate and the adsorbent [45]. This is also consistent with section 3.1. In addition, the Q_e of the adsorption process with the same initial F^- concentration increases significantly with the decrease of pH in the fitting of pseudo-second-order kinetics. This may be because F^- compete with OH^- for adsorption sites on calcium precipitate. F^- had a higher affinity than OH^- and the reaction occurred spontaneously.

Fig. 6((a) and (b)) show the adsorption isotherm of F^- by calcium precipitation. The experimental data of adsorption isotherm are presented in Table 2. The experimental results show that the adsorption process was more consistent with the Freundlich isotherm model (R^2>0.99) than the Langmuir isotherm model (R^2< 0.99) (Table 2). The calculated value of Q_m was quite different from the actual one, which also proved that the Langmuir model would not fit the process well. K_A and K_f both showed an increasing trend with the temperature increasing. It is possible that elevating the temperature increases the probability of molecular collisions and enhances the adsorption rate. Meanwhile, the constants (n) are all greater than 1 and increase with rising temperature, indicating that higher temperature favors the adsorption [9]. Langmuir isothermal adsorption model states that there is no interaction between adsorbents, so it can be concluded that adsorption activation energy, desorption activation energy, and adsorption heat are

independent of adsorption degree. In the real world, however, adsorption molecules interact with each other. The Freundlich isotherm assumes that the adsorbent surface is heterogeneous and the energy at each nucleation site is not uniform [34]. In fact, both the adsorption activation energy and the desorption energy are affected by the surface area covered by the adsorbent [46]. With the increase of covered area, the adsorption activation energy also increases. The desorption energy showed the opposite trend. Therefore, the adsorption heat inevitably decreased with the increase of the coverage rate [33]. Freundlich isotherms can be used for non-ideal adsorption and multilayer adsorption on heterogeneous surfaces [32]. The nucleation sites on the surface of microorganisms may be uneven, as is the calcium precipitation in the early stage of nucleation. Therefore, the adsorption process of calcium precipitation is not a single layer of uniform adsorption. The results of the adsorption isotherm experiment were also in accord with the principle of heterogeneous nucleation of biomineralization.

Based on this assumption, the empirical equation derived from the Freundlich model is more in line with the actual situation. The results of this experiment show that the adsorption process more closely fitted the Freundlich model than the Langmuir model. The increase in K_f fitted by the Freundlich model as the temperature rose suggested that the adsorption might be an endothermic process. The isothermal adsorption curves (Fig. 6(a) and (b)) at different temperatures (18, 30, and 42 °C) clearly show that compared with the lower temperature at the same equilibrium concentration, calcium precipitation at higher temperatures exhibits higher F^- adsorption capacity. Therefore, the removal rate of F^- increased as the temperature increased. Similarly, Gao et al. [47] also reached the same conclusion.

6. Adsorption Thermodynamics Analysis of F^- Removal

According to the results of the thermodynamic experiment of removing F^-, the thermodynamic parameters of the reaction at different temperatures were also obtained. The data of ΔG, ΔH, and ΔS of adsorption are shown in Table 3. We can see that ΔG is negative and decreases with increasing temperature, indicating that the adsorption process of the calcium precipitation to F^- is spontaneous and the temperature rise is beneficial to the adsorption process. When ΔH is greater than zero, the reaction is endothermic, and exothermic at below zero. The total entropy increases when the ΔS is greater than zero and decreases when it is less than zero. It can be seen (Table 3) that the changes in enthalpy and entropy of the reaction are both greater than zero. ΔH less than 40 kJ mol^{-1} indicates that the process may include physical adsorption, which is also consistent with section 3.5. The results suggest that the adsorption of F^- by calcium precipitation is an endothermic entropy reaction [48]. The results also provide a reasonable explanation for adsorption isothermal experiments. This is consistent with previous study of [47]. Moreover, ΔS greater than zero may mean that the randomness of the molecular motion at the solid-liquid interface has increased [49]. Both ΔH and ΔS are greater than 0, indicating that the entire adsorption process is not only physical adsorption but also accompanied by a chemical adsorption process. This part also supported by the previous results [44].

The activation energy (Ea) and the frequency factor (A) of the reaction could be calculated from the slope and intercept of the Arrhenius equation, respectively (Fig. 6(c)). After obtaining the activation energy and frequency factor, the reaction time required at different temperatures after adsorption equilibrium can be obtained by the Arrhenius equation. The experimental data show that the activation adsorption energy is 2.81 kJ mol^{-1} and the frequency factor is 10.88 h^{-1}.

CONCLUSIONS

Calcium precipitation induced by strain H12 was found to play an important role in the removal of F^- from water. Based on the study, different initial concentrations, pH, and temperature affected the removal ratio of F^-. The results demonstrated that the adsorption process highly conformed to pseudo-second-order. The adsorption isotherm at different temperatures indicated that heating would increase the adsorption capacity. According to the experimental results, the activation energy (2.81 kJ mol^{-1}) and the frequency factor (10.88 h^{-1}) were obtained by the Arrhenius equation. The experimental data of adsorption thermodynamics illustrated that the adsorption process was a spontaneous endothermic reaction. By three-dimensional fluorescence analysis, it was found that strain H12 could secrete EPS to change the solution environment and provide nucleation sites. By XRD and XPS analysis, it could be inferred that F^- adsorbed and co-precipitated via calcium precipitation. Based on these theoretical and experimental studies, the calcium precipitation induced by strain H12 has great potential in groundwater defluoridation.

ACKNOWLEDGEMENTS

This research work was partly supported by the National Natural Science Foundation of China, China (NSFC) (No. 51978556), Shaanxi Science Fund for Distinguished Young Scholars, China (No. 2019JC-31) and the Youth Innovation Team of Shaanxi Universities.

AUTHORSHIP CONFIRMATION STATEMENT

All authors contributed to the study conception and design. Conceptualization: **Junfeng Su**. Material preparation, data collection and analysis were performed by **Xiaofen Hu** and **Zhao Wang**. The first draft of the manuscript was written by **Ruijie Zhang** and

Table 3. Thermodynamic parameters of adsorption

ΔG (kJ $mole^{-1}$)			ΔH (kJ $mole^{-1}$)	ΔS (kJ $mole^{-1}$ K^{-1})
291.15 K	303.15 K	315.15 K		
−8.4283	−8.5874	−9.9854	2.8130	0.0199

all authors commented on previous versions of the manuscript. Writing - review & editing: **Amjad Ali**. All authors read and approved the final manuscript.

AUTHOR(S') DISCLOSURE STATEMENT(S)

No conflict of interest existed in the submission of this manuscript and it was approved by all authors for publication.

SUPPORTING INFORMATION

Additional information as noted in the text. This information is available via the Internet at http://www.springer.com/chemistry/journal/11814.

REFERENCES

1. S. Ayoob, A. K. Gupta and V. T. Bhat, *Crit. Rev. Env. Sci. Tec.*, **38**(6), 401 (2008).
2. P. Loganathan, S. Vigneswaran, J. Kandasamy and R. Naidu, *J. Hazard. Mater.*, **248-249**, 1 (2013).
3. WHO, n.d. Guidelines for Drinking-water Quality (2011).
4. M. Abtahi, S. Dobaradaran, S. Jorfi, A. Koolivand, S. S. Khaloo, J. Spitz, H. Saeed, N. Golchinpour and R. Saeedi, *Water. Res.*, **157**, 94 (2019).
5. A. A. Adenuga, O. D. Amos, J. A. O. Oyekunle and E. H. Umukoro, *J. Environ. Chem. Eng.*, **7**, 103317 (2019).
6. D. Kanduti, P. Sterbenk and B. Artnik, *Materia. Socio. Medica.*, **28**, 133 (2016).
7. A. Betancor-Abreu, V. F. Mena, S. González, S. Delgado, R. M. Souto and J. J. Santana, *J. Water Process. Eng.*, **31**, 100865 (2019).
8. M. Mourabet, A. El Rhilassi, H. El Boujaady, M. Bennani-Ziatni, R. El Hamri and A. Taitai, *J. Saudi Chem. Soc.*, **1**, 603 (2015).
9. M. Wang, X. Yu, C. Yang, X. Yang, M. Lin and L. Guan, *Chem. Eng. J.*, **322**, 246 (2017).
10. C. Ye, B. Yan, X. Ji, B. Liao, R. Gong, X. Pei and G. Liu, *Ecotoxicol. Environ. Saf.*, **180**, 366 (2019).
11. L. Deng, X. Zhang, T. Huang and J. Zhou, *J. Chem. Technol. Biotechnol.*, **94**, 569 (2019).
12. S. J. Bogart, S. Woodman, D. Steinkey, C. Meays and G. G. Pyle, *Sci. Total Environ.*, **559**, 182 (2016).
13. M. N. Sepehr, K. Yetilmezsoy, S. Marofi, M. Zarrabi, H. R. Ghaffari, M. Fingas and M. Foroughi, *J. Taiwan. Inst. Chem. E.*, **45**, 2786 (2014).
14. C. Liu, T. H. Chong, H. John, L. V. Fundamentals and L. Nanofiltration, *J. Membr. Sci.*, **521**, 18 (2018).
15. J. R. Liu, J. F. Su, A. Ali, Z. Wang and R. J. Zhang, *J. Hazard. Mater.*, **423**, 126976 (2022).
16. W. B. Lin, W. Lin, X. H. Cheng, G. Z. Chen and Y. C. Ersan, *Appl. Sci-Basel.*, **11**, 7842 (2021).
17. C. M. Heveran, S. L. Williams, J. Qiu, J. Artier, M. H. Hubler, S. M. Cook, J. C. Cameron and W. V. Srubar Iii, *Matter.*, **2**, 481 (2020).
18. N. K. Dhami, M. S. Reddy and M. S. Mukherjee, *Front. Microbiol.*, **4**, 1 (2013).
19. N. J. Jiang, R. Liu, Y. J. Du and Y. Z. Bi, *Sci. Total Environ.*, **672**, 722 (2019).
20. L. Cheng, T. Kobayashi and M. A. Shahin, *Constr. Build. Mater.*, **231**, 117095 (2020).
21. M. Oualha, S. Bibi, M. Sulaiman and N. Zouari, *J. Environ. Manage.*, **257**, 109965 (2020).
22. J. Shi, C. Xu and H. Han, *Bioresour. Technol.*, **298**, 122570 (2019).
23. H. H. Zhang, J. Feng, S. N. Chen, Z. F. Zhao, B. Q. Li, Y. Wang, J. Y. Jia, S. L. Li, Y. Wang, M. M. Yan, K. Y. Lu and H. Y. Hao, *Microb. Ecol.*, **77**, 304 (2019).
24. J. L. Arias and M. S. Fernández, *Chem. Rev.*, **108**, 4475 (2008).
25. T. Zhu and M. Dittrich, *Front. Bioeng. Biotechnol.*, **4**, 1 (2016).
26. S. Mukherjee, P. Sahu and G. Halder, *J. Environ. Manage.*, **204**, 413 (2017).
27. J. F. Su, H. Zhang, T. Huang, X. Hu, C. Chen and J. Liu, *Ecotoxicol. Environ. Saf.*, **187**, 109855 (2020).
28. J. F. Su, J. X. Shi, T. L. Huang and F. Ma, *Mar. Pollut. Bull.*, **109**, 87 (2016).
29. J. F. Su, Y. M. Zhang, D. H. Liang, J. X. Wang, Z. Wang and M. Li, *Bioresour. Technol.*, **286**, 121407 (2019).
30. J. F. Su, Y. H. Bai, T. L. Huang, L. Wei, C. Y. Gao and Q. Wen, *Water. Res.*, **168**, 115152 (2020).
31. L. T. Wang, Y. H. Xie, J. L. Yang, X. Q. Zhu, Q. L. Hu, X. Y. Li and Z. Liu, *Rsc. Adv.*, **7**, 54291 (2017).
32. F. Chi, S. Hu, J. Xiong and X. Wang, *Sci. China. Chem.*, **56**, 1495 (2013).
33. Y. H. Bai, J. Su, Q. Wen, G. Li, L. Xue and T. Huang, *Bioresour. Technol.*, **312**, 123565 (2020).
34. A. Abdurahman, K. Cui, J. Wu, S. Li, R. Gao, J. Dai and W. Liang, *Ecotoxicol. Environ. Saf.*, **198**, 110658 (2020).
35. M. Conde-cid, D. Fernández-calviño, A. Núñez-delgado and M. J. Fernández-sanjurjo, *Ecotoxicol. Environ. Saf.*, **196**, 110584 (2020).
36. L. Rao, J. Luo, W. Zhou, Z. Zou, L. Tang and B. Li, *Ecotoxicol. Environ. Saf.*, **202**, 110915 (2020).
37. S. Jiang, H. Pan, C. Yan, X. Xu and R. Tang, *Faraday Discuss.*, **179**, 451 (2015).
38. J. F. Su, Z. Z. Wu, T. L. Huang, H. Zhang and J. W. Li, *J. Hazard. Mater.*, **399**, 122846 (2020).
39. T. Zhu, C. Paulo, M. L. Merroun and M. Dittrich, *Ecol. Eng.*, **82**, 459 (2015).
40. S. Mukherjee and G. Halder, *J. Environ. Chem. Eng.*, **6**, 1257 (2018).
41. P. Anbu, C. H. Kang, Y. J. Shin and J. S. So, *SpringerPlus*, **5**, 250 (2016).
42. S. Dupraz, B. Ménez, P. Gouze, R. Leprovost, P. Bénézeth, O. S. Pokrovsky and F. Guyot, *Chem. Geol.*, **265**, 54 (2009).
43. N. N. N. Mahasti, Y. J. Shih, X. T. Vu and Y. H. Huang, *J. Taiwan Inst. Chem. Eng.*, **78**, 378 (2017).
44. Y. Li, X. Zhang, P. Zhang, X. Liu and L. Han, *J. Clean. Prod.*, **262**, 121350 (2020).
45. J. Prakash, C. Hsu, T. Lin, W. Lee and P. Bhattacharya, *Environ. Nanotechnol. Monit. Manag.*, **9**, 18 (2018).
46. D. Lu, S. Xu, W. Qiu, Y. Sun, X. Liu, J. Yang and J. Ma, *J. Clean. Prod.*, **264**, 121644 (2020).
47. S. Gao, R. Sun, Z. Wei, H. Zhao, H. Li and F. Hu, *J. Fluor. Chem.*, **130**, 550 (2009).
48. M. Niu, G. Li, L. Cao, X. Wang and W. Wang, *J. Clean. Prod.*, **256**, 120700 (2020).
49. S. V. Mousavi, A. Bozorgian, N. Mokhtari, M. A. Gabris, H. Rashidi Nodeh and W. A. Wan Ibrahim, *Microchem. J.*, **145**, 914 (2019).